Research Article – Vol. 02, Issue 03, No. 06

Advanced in Engineering and Intelligence Systems

Journal Web Page: https://aeis.bilijipub.com

Optimization and performance analysis of a geothermal-based power generation system based on flash-binary and dual-pressure evaporation organic Rankine cycles using zeotropic mixtures

Mojtaba Nedaei[1] Abolfazl keykhah[2,*] , borzo kamary[2], Ehsanolah Assareh [2,3]

[1] *Department of Management & Engineering, University of Padova, Vicenza, Italy*
[2] *Department of Mechanical Engineering, Dezful Branch, Islamic Azad University, Dezful, Iran*
3 School of Chemical Engineering, Yeungnam University, Gyeongsan 38541, South Korea

Highlights

- Integration of geothermal energy with D-ORC for efficient power generation.
- Perfluoropentane/butene identified as the best D-ORC working fluid, yielding high efficiency.
- Positive economic indicators with a net present value of $10.85 million and a short payback period of 3.47 years.
- Identification of key components contributing to exergy destruction, aiding system optimization.

Article Info

Received: 29 July 2023
Received in revised: 10 September 2023
Accepted: 26 September 2023
Available online: 30 September 2023

Keywords

Single-flash geothermal system;
Dual-pressure organic Rankine cycle;
Zeotropic mixture;
Multi-objective optimization;
the net present value

Abstract

Population growth worldwide in recent decades has increased the demand for power. Geothermal energy provides a reliable and stable reservoir for power generation. This paper proposes an integration of single-flash geothermal with a dual-evaporation organic Rankine cycle (D-ORC) to generate power. The system's performance is estimated via thermodynamic and thermoeconomic analyses. Five different zeotropic mixtures are considered the D-ORC working fluid, and their performance is compared at the optimum state. Perfluoropentane/butene presents the best performance indexes and is considered the D-ORC's working fluid. Hence, the proposed system provides 7992.29 kW of net power with 62.42% exergetic efficiency. Also, the exergoeconomic performance indicates that the net present value and payback period are about 10.85 million dollars and 3.47 years, respectively. Also, the net present value of the proposed system is estimated for the four electricity sale and geofluid prices and reveals that the product sale costs influence the system's economic performance more than the purchase cost. The exergy destruction distribution in the employed components is shown as the Grassmann diagram. The steam turbine has the highest exergy destruction of about 996 kW, and the first expansion valve with 714 kW of exergy destruction is the next one. Also, the condensers contain considerable exergy destruction, about 26.98% of total exergy destruction.

Nomenclature

c	*Cost per exergy unit* $[\$.GJ^{-1}]$	$\dot{W}$	*Power* $[kW]$
CRF	*Capital Recovery Factor*	Z	*Investment cost of components* $[\$]$
DORC	*Dual Evaporation Organic Rankine Cycle*	***Subscript and abbreviations***	
e	*Specific Exergy* $[kJ.kg^{-1}]$	*Cond*	*Condenser*
$\dot{E}$	*Exergy rate* $[kW]$	*cr*	*Critical*
$\dot{E}x$	*Exergy flow* $[kW]$	*D*	*Destruction*
h	*Enthalpy* $[kJ.kg^{-1}]$	*Elec*	*Electrical*
Hx	*Heat Exchanger*	*EV*	*Expansion Valve*
K	*Interest rate [%]*	*in*	*Inlet*

* Corresponding Author: Abolfazl keykhah
Email: Abolfazl_keykhah@yahoo.com

$\dot{m}$	*Mass Rate* $[kg.s^{-1}]$	*is*	*Isentropic*
M M	*Molar Mass* $[g.mole^{-1}]$	*HPP*	*High Pressure Pump*
Mix	*Mixer*	*HPT*	*High Pressure Turbine*
NPV	*Net Present Value* [$]	*LPP*	*Low-Pressure Pump*
O&M	*Operation and Maintenance*	*LPT*	*Low-Pressure Turbine*
ORC	*Organic Rankine Cycle*	*PPT*	*Pinch Point Temperature [K]*
P	*Pressure [kPa]*	*sep*	*Separator*
PEC	*Purchased Equipment Cost [$]*	*out*	*Outlet*
Pu	*Pump*	*V.G*	*Vapor Generator*
Q	*Heat* $[kJ]$	0	*Dead State*
s	*Entropy* $[kJ.kg^{-1}.K^{-1}]$	1,2,3, …	*State Point*
ST	*Steam turbine*	***Greek symbols***	
t	*Time* [***s***]	η	*Efficiency*
T	*Temperature* $[K]$	φ	*Maintenance Factor*

1. Introduction

Besides lifestyle modernization, the worldwide population growth in recent decades has increased power demand. Hence, power's role in society's progress is considerable [1]. The central portion of the power demand is supplied by fossil fuels [2]. However, fossil fuel consumption in power systems leads to environmental pollution and CO2 emissions [3]. Therefore, governments, by authorizing restrictive laws, try to minimize their environmental effects [4]. So, investigating energy reservoirs for substituting fossil fuels, which includes zero environmental issues, refers to introducing renewable energies [5]. Although renewable energies have zero environmental topics, climate conditions highly affect their performance, except geothermal energy. So, geothermal energy prepares a reliable and sustainable reservoir to generate power [6]. The geothermal sources based on geofluid temperature are utilized in the different arrangements. Low-temperature reservoirs (under 90 ˚C) are used as the heat source in the power systems. Moderate temperatures (90-150 C) are used primarily in flash-binary systems, and high temperatures (higher than 150 C) are directly used to generate power [7]. The high-temperature reservoirs are scared, and most of the probed geothermal reservoirs contain moisture steam and are categorized as moderate-temperature [8]. Hence, various studies have been conducted to evaluate the geothermal-based power system's performance.

2. Literature review

Guzovic et al. [9] proposed a flash-binary geothermal power system with a Kalina and an ORC subsystem for a geothermal reservoir in Croatia. They studied their proposed system from a thermodynamic perspective and showed that utilizing the ORC subsystem presented 6% more power. Luo et al. [10] proposed different configurations of the geothermal power system for various discovered geothermal reservoirs in China. According to their results, the binary power presents higher thermodynamic performance than other considered configurations for low-temperature reservoirs, and the flash-binary type is proper for high-temperature reservoirs from a thermodynamic viewpoint. Yari [11] considered different configurations of geothermal power systems for a geothermal reservoir with a 130 ˚C temperature and showed that the flash-binary type presents the highest energy and exergetic efficiency. Then, he applied different ORC arrangements to the flash-binary system. Applying the ORC subsystem referred to increasing the proposed system performance, and among the considered ORC arrangements, the ORC subsystem with regenerative power presents the highest thermodynamic performance. Abdolalipouradl et al. [12] proposed different arrangements of the flash-binary system for the Sabalan geothermal field in Iran and studied their proposed systems from energy, exergy, and exergoeconomic assessments. Their results indicated that the double-flash system presents the highest net output power, while the single-flash system presents the best exergoeconomic performance. In the other study, Bina et al. [13] proposed a flash-binary system for the Sabalan geothermal field in Iran with different ORC configurations. They applied multi-objective optimization to their proposed systems and compared them from an exergoeconomic perspective. They showed that the ORC subsystem with an internal heat exchanger has the highest exergoeconomic performance at the optimum state. Pamudi et al. [14] studied a single-flash and a double-flash binary system for the Dieng geothermal field in Indonesia based on thermodynamic and thermoeconomic assessments. Based on their results, the double-flash system presents higher thermodynamic performance, and the single-flash system has a lower payback period. Pasek et al. [15] proposed a flash-binary system with an ORC subsystem for a moderate-temperature geothermal reservoir. Then, they performed a comparative study of thermodynamic performance to select the ORC system's working fluid. They showed that isopentane presents the highest net power and exergetic efficiency. Reviewing the studies reveals that the geothermal system includes considerable wasted energy

like the other power systems. Hence, applying subsystems to the geothermal system enhances the proposed system's performance. Also, ORC is the most desirable subsystem for geothermal systems. Shokati et al. [16] proposed simple-ORC and dual-pressure ORC subsystems to recover a geothermal power system. They showed that the DORC subsystem presents 15.7% higher net power compared to the single-pressure ORC subsystem. Franco et al. [17] compared single-pressure and dual-pressure ORC systems performance from an energy perspective and showed that the dual-pressure ORC provides 15% more net power and 21% higher thermal efficiency than the single-pressure ORC with the same heat source temperature. Peris et al. [18] performed a comparative study of the ORC system's six single-pressure and dual-pressure arrangements based on thermodynamic performance. Their results revealed that applying a regenerative unit to the ORC improves system performance, and the dual-pressure ORC with a regenerative unit contains an 8% higher thermal efficiency than the single-pressure ORC with a regenerative unit. The ORC subsystems studied in the previous papers utilized a pure substance as the working fluid. Since the ORC system contains the constant-temperature evaporation process at their vapor generator unit. This phase change includes considerable exergy destruction through the temperature mismatch. To reduce these disadvantages, zeotropic mixture utilization in the ORC subsystems is suggested [19]. These mixtures include two or more substances with different evaporation points, so during the phase change in the heat exchanger, the mixture temperature varies, and the exergy destruction and the temperature mismatch in the heat exchanger are considerably solved [20]. Li et al. [21] studied the impact of the zeotropic mixture and pure substance utilization on an ORC system's performance. They showed that utilizing the zeotropic mixture enhanced their ORC system's performance considerably. Zhao et al. [22] performed an experimental study investigating the zeotropic mixture of R245fa/R152fa and the pure substance of R245fa's performance from an energy assessment. Their results indicated that the considered zeotropic mixture at the 0.7-0.3 mass fraction represented considerably higher performance than the pure substance. Tian et al. [2] compared different zeotropic mixtures in a dual-pressure organic Rankine cycle (DORC) based on thermodynamic and economic assessments. Their results revealed that the D4/R123 zeotropic mixture presents the highest thermodynamic performance, and the MD2M/R123 zeotropic mixture provides the best economic performance among considered zeotropic mixtures.

2.1.Main contribution and novelties

Reviewing the previous studies shows that the flash-binary system is the best configuration for the moderate-temperature geothermal reservoir, and the dual-pressure ORC with zeotropic mixture working fluid presents the highest performance to recover the geothermal power system's waste energy. Hence, this paper proposes a single-flash binary geothermal power system with a DORC subsystem to generate power. The first and second laws of thermodynamic and exergoeconomic analysis are conducted to obtain the performance indexes of the designed system. Also, the following novelties are considered in this paper:

- Dual-pressure ORC with zeotropic working fluid has been employed to recover the waste energy of the geothermal power system.
- Multi-objective optimization has been applied to the proposed system to obtain its optimum operational condition.
- Six different zeotropics have been employed to compare and select the best working fluid for the DORC subsystem.
- The zeotropic mixtures performance comparison has been conducted at the system's optimum state.
- The net present value of the proposed system is estimated at four different prices.
- The exergy destruction distribution is shown as the Grassmann diagram.

2.2. Paper structure

This paper contains different sections that demonstrate applied studies on the proposed system and are categorized as the following:

Section 2 demonstrates the system's operation mode and the flows' directions that cross the components. Section 3 illustrates the assumptions and input data employed to simulate the proposed system. Then, applied mass, energy, exergy, and exergoeconomic analyses are presented in Tables 3 and 4. Also, a validation of the simulation with Wang et al. [23] data is conducted in Section 4 to evaluate the results' accuracy. Section 5 presents the paper results, and this section contains different subsections. In Section 5.1, multi-objective optimization is applied to the system, in which six different zeotropic mixtures are employed as the DORC subsystem working fluid. The next subsection compares the results of employing various working fluids to select a proper working fluid for the D-ORC subsystem. Then, the net present value of the proposed system is estimated for the four price scenarios in Section 5. 3. Also, the distribution of the exergy destruction in the proposed

system components is presented in Section 5. 4. Finally, the overall conclusion of this paper is illustrated in Section 6.

3. System description

Fig. 1 illustrates the schematic diagram of the proposed system. The geo-fluid is extracted from underground (state 1) and crosses the expansion valve (state 2). The geo-fluid becomes two-phase in the expansion valve and enters the separator unit (state 2). During the flash process in the separator unit, the vapor part is led to a steam turbine (state 3) to expand and generate power. After crossing the turbine, the geo-fluid enters the Condenser 1 unit and cools down (state 4). On the other hand, the liquid part of the geo-fluid exits the separator unit. It crosses the vapor generators 1 and 2 and Hx units to transfer the energy to the DORC subsystem, respectively (states 9-12). Then, the geofluid crosses the second expansion and is mixed with the Condenser 1 outlet flow in the mixer. Finally, it brines underground (state 8).

In the DORC subsystem, the zeotropic working fluid of the DORC subsystem is pressurized in the low-pressure pump and becomes a sub-cooled liquid, then enters the Hx unit (state 20) and is preheated by geo-fluid to reach saturated liquid (state 21). Then, divide into two parts. The first part is led to the vapor generator 2 unit (state 23), and the second is to the high-pressure pump (state 22). In the high-pressure pump unit, the zeotropic fluid is pressurized and becomes sub-cooled liquid, which then enters the vapor generator 1 unit (state 25). In the vapor generator 1 unit, the high-pressure fluid becomes saturated vapor and exits to the high-pressure turbine (state 15). The saturated vapor is expanded in the HP turbine, generates power, and leaves the turbine in a superheated vapor state (state 16). The high-pressure turbine outlet flow is mixed with the vapor generator 2 outlet flow (state 24). The mixture flow in the superheated state enters the LP turbine (state 17). After expanding the process in the LP turbine unit, the zeotropic flow enters Condenser 2 (state 18) and is then led to the low-pressure pump unit to complete the cycle.

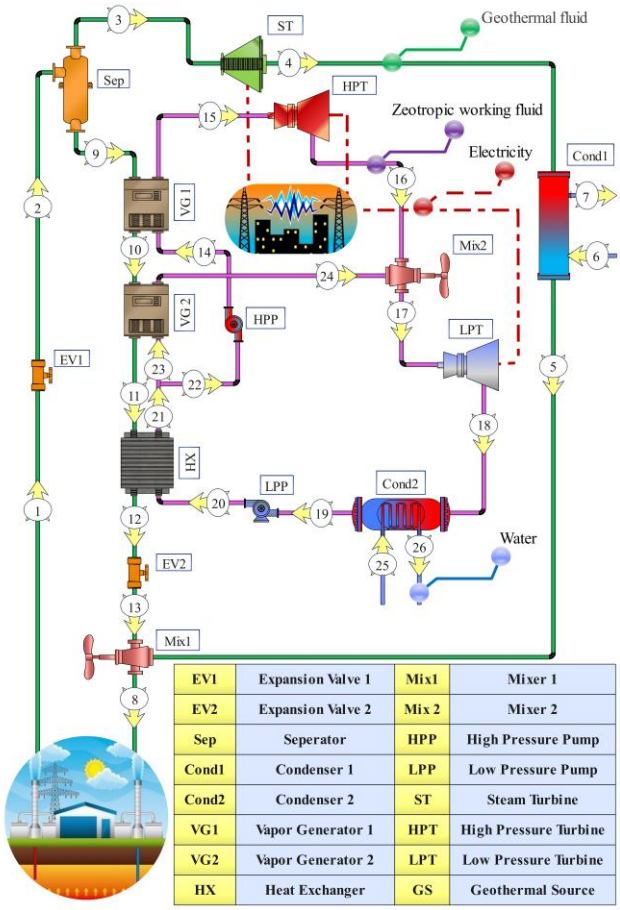

Fig. 1. The schematic diagram of the proposed system.

4. Mathematical modeling

This section discusses the mass, energy, exergy, and exergoeconomic equations that govern all components. To simplify the system's simulation, the following assumptions are taken into account:

- All components operate in steady-state mode [24].
- The change in kinetic and potential energies is negligible [24].
- The pressure drop in pipelines and heat exchangers is not considered [25].
- All components are adiabatically designed to prevent heat loss to the ambient [25].
- All turbines and pumps work at certain isentropic efficiencies [26].
- The throttling process in the expansion valve is assumed to be isenthalpic [26].

Also, the physical properties of selected working fluids and main input parameters are presented in Tables 1 and 2, respectively.

Table 1. The main characteristics of the employed fluids in this work.

Fluid	T_{cr} [K]	P_{cr} [kPa]	MM [$kg.kmol^{-1}$]	Type [$dT.ds^{-1}$]
Pentane	469.7	3370	72.15	dry
Isopentane	460.35	3378	72.15	dry
Perfluoropentane	420.56	2045	288.03	dry
Butene	419.29	4005.1	56.11	dry
Butane	425.13	3796	58.12	dry
Cis-2-butene	435.75	4225.5	56.11	dry
Trans-2-butene	428.61	4027.3	56.11	dry
Hexane	507.82	3034	86.18	dry

Table 2. Some of the input parameters and assumptions.

Parameter	symbol	Value	unit
Reference temperature	T_0	293.15	[K]
Reference pressure	P_0	101	[kPa]
Geothermal fluid mass flow rate	$\dot{m}_1$	60	[$kg.s^{-1}$]
Geothermal fluid enthalpy	h_1	1000.	[$kJ.kg^{-1}$]
Geothermal fluid pressure	P_1	1200000(	[kPa]
Steam turbine isentropic efficiency	$\eta_{is,ST}$	85.	[%]
ORC turbine isentropic efficiency	$\eta_{is,Tur}$	85.	[%]
ORC pump isentropic efficiency	$\eta_{is,Pump}$	85.	[%]
Pinch point temperature difference of the condenser	$\Delta T_{PPT,Cond}$	10	[K]
Pinch point temperature difference of the vapor generator	$\Delta T_{PPT,VG}$	15.	[K]

4.1.Mass and energy balance

The mass and energy1balance relations at the1steady-state with neglecting the kinetic1and1potential energies change, could be written as [27]:

$$\sum \dot{m}_{in} = \sum \dot{m}_{out} \quad (1)$$

$$\dot{Q} - \dot{W} = \sum \dot{m}_{out} h_{out} - \sum \dot{m}_{in} h_{in} \quad (2)$$

$\dot{m}$ is the mass rate, $\dot{Q}$ depicts the heat transfer from the control volume's borders, $\dot{W}$ demonstrates output work, and h indicates the specific enthalpy.

4.2. Exergy balance

The exergy balance at the steady state is given by [27]:

$$\dot{E}_Q - \dot{W} = \sum \dot{m}_{out} e_{out} - \sum \dot{m}_{in} e_{in} + \dot{E}_D \quad (3)$$

where $\dot{E}_D$ determines the exergy destruction rate. Also, $\dot{E}_Q$ is the net exergy transfer that can be calculated by [27]:

$$\dot{E}_Q = \sum \dot{Q} \left(1 - \frac{T_0}{T}\right) \quad (4)$$

which T denotes the temperature. As well, T_0 refers to the dead-state temperature. The exergy low can be presented as follows [27]:

$$e = h - h_0 - T_0(s - s_0) \quad (5)$$

which s refers to the specific entropy. The first and second laws of thermodynamics equations are illustrated in Table 3 to summarize the applied thermodynamic analysis to the system's components.

Table 3. Mass, energy, and exergy balance equation for components.

Component	Mass balance	Energy balance	Exergy balance
Expansion valve 1	$\dot{m}_1 = \dot{m}_2$	$\dot{m}_1 h_1 = \dot{m}_2 h_2$	$\dot{E}_D^{EV1} = \dot{E}_1 - \dot{E}_2$
Separator	$\dot{m}_2 = \dot{m}_3 + \dot{m}_9$	$\dot{m}_2 h_2 = \dot{m}_3 h_3 + \dot{m}_9 h_9$	$\dot{E}_D^{Sep} = \dot{E}_2 - (\dot{E}_3 + \dot{E}_9)$
Steam turbine	$\dot{m}_3 = \dot{m}_4$	$\dot{W}_{ST} = \dot{m}_3 h_3 - \dot{m}_4 h_4 = (\dot{m}_3 h_3 - \dot{m}_4 h_{4s})\eta_{is,ST}$	$\dot{E}_D^{ST} = (\dot{E}_3 - \dot{E}_4) - \dot{W}_{ST}$
Vapor generator 1	$\dot{m}_9 = \dot{m}_{10}$, $\dot{m}_{14} = \dot{m}_{15}$	$\dot{Q}_{VG1} = \dot{m}_9 h_9 - \dot{m}_{10} h_{10} = \dot{m}_{15} h_{15} - \dot{m}_{14} h_{14}$	$\dot{E}_D^{VG1} = (\dot{E}_9 - \dot{E}_{10}) - (\dot{E}_{15} - \dot{E}_{14})$
Vapor generator 2	$\dot{m}_{10} = \dot{m}_{11}$, $\dot{m}_{23} = \dot{m}_{24}$	$\dot{Q}_{VG2} = \dot{m}_{10} h_{10} - \dot{m}_{11} h_{11} = \dot{m}_{24} h_{24} - \dot{m}_{23} h_{23}$	$\dot{E}_D^{VG1} = (\dot{E}_{10} - \dot{E}_{11}) - (\dot{E}_{24} - \dot{E}_{23})$
Heat exchanger	$\dot{m}_{11} = \dot{m}_{12}$, $\dot{m}_{20} = \dot{m}_{21}$	$\dot{Q}_{Hx} = \dot{m}_{11} h_{11} - \dot{m}_{12} h_{12} = \dot{m}_{21} h_{21} - \dot{m}_{20} h_{20}$	$\dot{E}_D^{Hx} = (\dot{E}_{11} - \dot{E}_{12}) - (\dot{E}_{21} - \dot{E}_{20})$
Expansion valve 2	$\dot{m}_{12} = \dot{m}_{13}$	$\dot{m}_{12} h_{12} = \dot{m}_{13} h_{13}$	$\dot{E}_D^{EV1} = \dot{E}_{12} - \dot{E}_{13}$
High pressure turbine	$\dot{m}_{15} = \dot{m}_{16}$	$\dot{W}_{HPT} = \dot{m}_{15} h_{15} - \dot{m}_{16} h_{16} = (\dot{m}_{15} h_{15} - \dot{m}_{16} h_{16s})\eta_{is,Tur}$	$\dot{E}_D^{HPT} = (\dot{E}_{15} - \dot{E}_{16}) - \dot{W}_{HPT}$
Low pressure turbine	$\dot{m}_{17} = \dot{m}_{18}$	$\dot{W}_{LPT} = \dot{m}_{17} h_{17} - \dot{m}_{18} h_{18} = (\dot{m}_{17} h_{17} - \dot{m}_{18} h_{18s})\eta_{is,Tur}$	$\dot{E}_D^{LPT} = (\dot{E}_{17} - \dot{E}_{18}) - \dot{W}_{LPT}$
Condenser 1	$\dot{m}_4 = \dot{m}_5$, $\dot{m}_6 = \dot{m}_7$	$\dot{Q}_{Cond1} = \dot{m}_4 h_4 - \dot{m}_5 h_5 = \dot{m}_7 h_7 - \dot{m}_6 h_6$	$\dot{E}_D^{Cond1} = (\dot{E}_4 - \dot{E}_5) - (\dot{E}_7 - \dot{E}_6)$
Mixer 1	$\dot{m}_{17} = \dot{m}_{16} + \dot{m}_{24}$	$\dot{m}_{17} h_{17} = \dot{m}_{16} h_{16} + \dot{m}_{24} h_{24}$	$\dot{E}_D^{Mixer1} = (\dot{E}_{16} + \dot{E}_{24}) - \dot{E}_{17}$
Mixer 2	$\dot{m}_8 = \dot{m}_5 + \dot{m}_{13}$	$\dot{m}_8 h_8 = \dot{m}_5 h_5 + \dot{m}_{13} h_{13}$	$\dot{E}_D^{Mixer2} = (\dot{E}_5 + \dot{E}_{13}) - \dot{E}_8$
Condenser 2	$\dot{m}_{18} = \dot{m}_{19}$, $\dot{m}_{25} = \dot{m}_{26}$	$\dot{Q}_{Cond,2} = \dot{m}_{18} h_{18} - \dot{m}_{19} h_{19} = \dot{m}_{26} h_{26} - \dot{m}_{25} h_{25}$	$\dot{E}_D^{Cond2} = (\dot{E}_{18} - \dot{E}_{19}) - (\dot{E}_{26} - \dot{E}_{25})$
High pressure pump	$\dot{m}_{22} = \dot{m}_{14}$	$\dot{W}_{HPP} = \dot{m}_{14} h_{14} - \dot{m}_{22} h_{22} = (\dot{m}_{14} h_{14s} - \dot{m}_{22} h_{22})/\eta_{is,Pump}$	$\dot{E}_D^{HPP} = \dot{W}_{HPP} - (\dot{E}_{14} - \dot{E}_{22})$
Low pressure pump	$\dot{m}_{20} = \dot{m}_{19}$	$\dot{W}_{LPP} = \dot{m}_{20} h_{20} - \dot{m}_{19} h_{19} = (\dot{m}_{20} h_{20s} - \dot{m}_{19} h_{19})/\eta_{is,Pump}$	$\dot{E}_D^{LPP} = \dot{W}_{LPP} - (\dot{E}_{20} - \dot{E}_{19})$

4.3. Exergoeconomic analysis

The power system analyses based on thermodynamics' first and second laws show the energy and exergy performance assessments. These approaches do not satisfy the system's performance in all aspects. Applying the thermoeconomic analysis can be helpful to cover this gap. Hence, the economic relations are applied to the system's exergy balances to illustrate the exergoeconomic performance. The first economic equation is the cost balance, which is applied to the employed components and demonstrated as [28]:

$$\dot{C}_{q,k} + \sum \dot{C}_{in,k} + \dot{Z}_k = \dot{C}_{w,k} + \sum \dot{C}_{out,k} \quad (6)$$

where;

$$\dot{C} = c\dot{E}x \quad (7)$$

Also, the input and output exergies ($\dot{E}x_{in}$,$\dot{E}x_{out}$) are defined as power ($\dot{E}x_w$) and heat transfer ($\dot{E}x_q$), and their unit costs are calculated as [28]:

$$\dot{C}_{in} = c_{in}\dot{E}x_{in} = c_{in}(\dot{m}_{in}ex_{in}) \quad (8)$$

$$\dot{C}_{out} = c_{out}\dot{E}x_{out} = c_{out}(\dot{m}_{out}ex_{out}) \quad (9)$$

$$\dot{C}_w = c_w\dot{E}x_w = c_w(\dot{m}_w ex_w) \quad (10)$$

$$\dot{C}_q = c_w\dot{E}x_q = c_q(\dot{m}_q ex_q) \quad (11)$$

In (8)-(11), Ċ and c depict the cost rate and unit exergy cost, respectively.

The exergy destruction cost rate in the components is defined as [28]:

$$\dot{C}_{D,k} = c_{P,k}\dot{E}x_{D,k} \quad (12)$$

The component k's total cost consists of the capital cost and the operation and maintenance costs (cost summation) [28]:

$$\dot{Z}_k = \dot{Z}^{CI} + \dot{Z}^{OM} \quad (13)$$

which $\dot{Z}^{CI}$ is the capital cost, and $\dot{Z}^{OM}$ denotes the operation and maintenance cost. Another economic analysis criteria is the annual investment cost, which is

calculated based on the component's total cost and estimated from the following [29]:

$$Z_k = \frac{CRF \times \varphi}{N \times 3600} \times \dot{Z}_k \quad (14)$$

which Z_k depicts the purchasing cost of the component, N refers to the annual operating time and is assumed to be 3960 hours, φ defines the maintenance factor and is considered to be 1.06, and CRF is the capital recovery factor, which is obtained from (15) [28]:

$$CRF = \frac{i(1+i)^n}{(1+i)^n - 1} \quad (15)$$

where i stands for the interest rate and is equal to 0.15. n, which demonstrates the components designed lifetime and is considered 20 years.

Also, the products' total cost rate is illustrated as the product cost summation and calculated as [28]:

$$\dot{c}_{tot} = \Sigma \dot{c}_p \quad (16)$$

The cost data belong to the reference date, and to express the proposed system's economic performance, these data should be updated for the designed year. This update is conducted via the chemical cost index, whose value for the 2020 date is about 668. In this way, the updated cost is estimated as [28]:

$$\text{Cost in target year} = \text{cost in reference year} \times \frac{\text{Cost index of target year}}{\text{Cost index of reference year}} \quad (17)$$

The net present value (NPV) is another economic analysis index that converts the following year's cost to the present through the interest rate. Also, this index illustrates the system's profitability and includes the payback period estimation. Hence, the NPV calculation helps the designers and investors draw the system's economic roadmap. The NPV index is obtained from [28]:

$$NPV_n = -(FC) + \sum_{n=0}^{n} Y(1+i)^{-n} \quad (18)$$

FC stands for the fixed cost and is the component purchase costs' summation, and Y is the net cash flow [28]:

$$Y = AI - \left(C^{O\&M} + C_f\right) \quad (19)$$

The C_f depicts the fuel cost, which in the current study is zero because the sun supplies the proposed system's fuel. Also, AI is the annual income and is estimated as [28]:

$$AI = \mathrm{AI} = \mathrm{c_{elec}} \times \mathrm{t_{year}} \times \dot{\mathrm{W}}_{\mathrm{net}} + \mathrm{c_{cool}} \times \mathrm{t_{year}} \times \dot{\mathrm{Q}}_{\mathrm{cool}} \quad (20)$$

$$C^{O\&M} = 0.06 \times FC \quad (21)$$

$$C_f = 0 \quad (22)$$

As mentioned, the NPV estimation leads to obtaining the system's payback period, which is defined as [28]:

$$PP = min\{n: NPV(n) > 0\} \quad (23)$$

The cost balance, cost function, and auxiliary equations of each component are presented in Table 4.

Table 4. Cost function, cost balance and auxiliary equations for components

Components	*Cost functions*	*Cost balance*	*Auxiliary equations*
Expansion valve 1	$PEC_{EV1} = 114.5 \times \dot{m}_1$	$\dot{C}_1 + \dot{Z}_{EV1} = \dot{C}_2$	$-$
Separator	$PEC_{Sep} = 0$	$\dot{C}_2 + \dot{Z}_{Sep} = \dot{C}_3 + \dot{C}_9$	$c_3 = c_9$
Steam turbine	$PEC_{ST} = 3880.5 \times \dot{W}_{ST}^{0.7}\left(1 + \left(\frac{0.05}{0.92 - \eta_{is,ST}}\right)^3\right)\left(1 + 5 \times 2.71^{\frac{(T_3 - 866)}{10.42}}\right)$	$\dot{C}_3 + \dot{Z}_{ST} = \dot{C}_4 + \dot{C}_{W,ST}$	$c_3 = c_4$
Vapor generator 1	$PEC_{VG1} = 17500\left(\frac{A_{VG1}}{100}\right)^{0.6}$	$\dot{C}_9 + \dot{C}_{14} + \dot{Z}_{VG1} = \dot{C}_{10} + \dot{C}_{15}$	$c_9 = c_{10}$
Vapor generator 2	$PEC_{VG2} = 17500\left(\frac{A_{VG2}}{100}\right)^{0.6}$	$\dot{C}_{10} + \dot{C}_{23} + \dot{Z}_{VG2} = \dot{C}_{11} + \dot{C}_{24}$	$c_{10} = c_{11}$
Heat exchanger	$PEC_{Hx} = 17500\left(\frac{A_{Hx}}{100}\right)^{0.6}$	$\dot{C}_{11} + \dot{C}_{20} + \dot{Z}_{Hx} = \dot{C}_{12} + \dot{C}_{21}$	$c_{11} = c_{12}$
Expansion valve 2	$PEC_{EV2} = 114.5 \times \dot{m}_{12}$	$\dot{C}_{12} + \dot{Z}_{EV2} = \dot{C}_{13}$	$-$
High pressure turbine	$PEC_{HPT} = 4750\left(\dot{W}_{HPT}\right)^{0.75}$	$\dot{C}_{15} + \dot{Z}_{HPT} = \dot{C}_{16} + \dot{C}_{W,HPT}$	$c_{15} = c_{16}$
Low pressure turbine	$PEC_{LPT} = 4750\left(\dot{W}_{LPT}\right)^{0.75}$	$\dot{C}_{17} + \dot{Z}_{LPT} = \dot{C}_{18} + \dot{C}_{W,HPT}$	$c_{17} = c_{18}$

Condenser 1	$PEC_{Cond1} = 8000\left(\frac{A_{Cond1}}{100}\right)^{0.6}$	$\dot{C}_4 + \dot{C}_6 + \dot{Z}_{Cond1} = \dot{C}_5 + \dot{C}_7$	$c_6 = 0, c_4 = c_5$
Mixer 1	$PEC_{Mixer1} = 0$	$\dot{C}_{16} + \dot{C}_{24} + \dot{Z}_{Mixer1} = \dot{C}_{17}$	–
Mixer 2	$PEC_{Mixer2} = 0$	$\dot{C}_5 + \dot{C}_{13} + \dot{Z}_{Mixer2} = \dot{C}_8$	–
Condenser 2	$PEC_{Cond2} = 8000\left(\frac{A_{Cond2}}{100}\right)^{0.6}$	$\dot{C}_{18} + \dot{C}_{25} + \dot{Z}_{Cond2} = \dot{C}_{19} + \dot{C}_{26}$	$c_{25} = 0, c_{18} = c_{19}$
High pressure pump	$PEC_{HPP} = 200(\dot{W}_{HPP})^{0.65}$	$\dot{C}_{22} + \dot{Z}_{HPP} + \dot{C}_{W,HPP} = \dot{C}_{14}$	–
Low pressure pump	$PEC_{LPP} = 200(\dot{W}_{LPP})^{0.65}$	$\dot{C}_{19} + \dot{Z}_{LPP} + \dot{C}_{W,LPP} = \dot{C}_{20}$	–

4.4. *Performance criteria*

In this section, the performance criteria of the proposed cases of study have been studied. The net power production at DORC subsystems and the whole system is calculated as follows:

$$\dot{W}_{DORC} = (\dot{W}_{HPT} + \dot{W}_{LPT}) - (\dot{W}_{LPP} + \dot{W}_{HPP}) \quad (26)$$

$$\dot{W}_{tot} = (\dot{W}_{ST} + \dot{W}_{LPT} + \dot{W}_{HPT}) - (\dot{W}_{LPP} + \dot{W}_{HPP}) \quad (27)$$

Also, the energy and exergetic efficiency of the ORC subsystem and whole system are estimated from (28)-(31):

$$\eta_{energy,DORC} = \frac{\dot{W}_{DORC}}{\dot{m}_9 \times (h_9 - h_{12})} \quad (28)$$

$$\eta_{energy,tot} = \frac{\dot{W}_{tot}}{\dot{m}_1 \times (h_1 - h_8)} \quad (29)$$

$$\eta_{exergy,DORC} = \frac{\dot{W}_{DORC}}{\dot{E}_9 - \dot{E}_{12}} \quad (30)$$

$$\eta_{exergy,tot} = \frac{\dot{W}_{tot}}{\dot{E}_1 - \dot{E}_8} \quad (31)$$

5. Validation

The first and second laws of thermodynamic analysis are applied to all study cases via the ESS code. Before presenting the obtained results, the flash separator tank's simulation is endorsed by Wang et al. [23]. The flash separator tank simulation validation is conducted by comparing the turbine's outlet power at different flashing pressures, as illustrated in Fig. 2, which are in good accuracy and validate the conducted simulation.

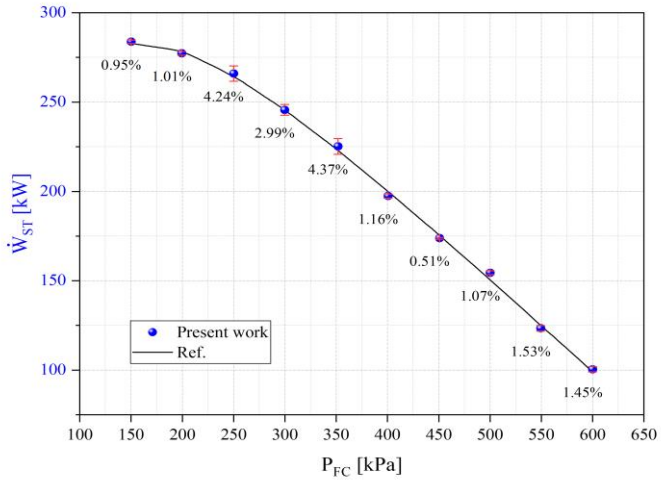

Fig. 2. The validation of flash cycle simulation with Wang et al. [23]

6. Results and discussion

6.1.Optimization

A multi-objective particle swarm optimization (MOPSO) is conducted to obtain the optimum condition of system performance. The optimization variables are selected for the separator inlet pressures, DORC subsystem vapor generators 1 and 2 evaporation temperatures, and the zeotropic mixture mass fraction. The payback period with exergetic efficiency is considered the cost function of optimization. The MOPSO method of employment performs a Pareto-frontier analysis of the optimum states. Hence, the optimum point is selected through these points, and an LINMAP code is utilized to select the final optimum state.

The zeotropic mixtures that were selected as the case study are: isopentane/butane, pentane/butane, pentane/cis-2-butene, pentane/hexane, pentane/trans-2-butene, and perfluoropentane/butene. Hence, the optimization is conducted via the mentioned zeotropic

mixtures as the DORC working fluid. Figs. 3–8 illustrate the optimization results. The optimum state comparison demonstrates that utilizing perfluoropentane/butene as the DORC working fluid presents the highest exergetic efficiency and the lowest payback period, about 62.42% and 3.47 years, respectively. The next one is pentane/butane, which presents 62.41% exergetic efficiency and a 3.49-year payback period. Also, isopentane/butane have the lowest exergetic efficiency and the highest payback period, about 61.76% and 3.58 years, respectively.

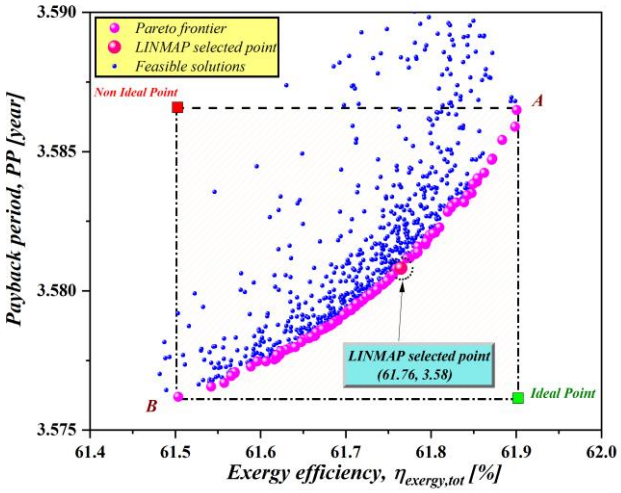

Fig. 3. The Isopentane/Butane zeotropic mixture optimization result.

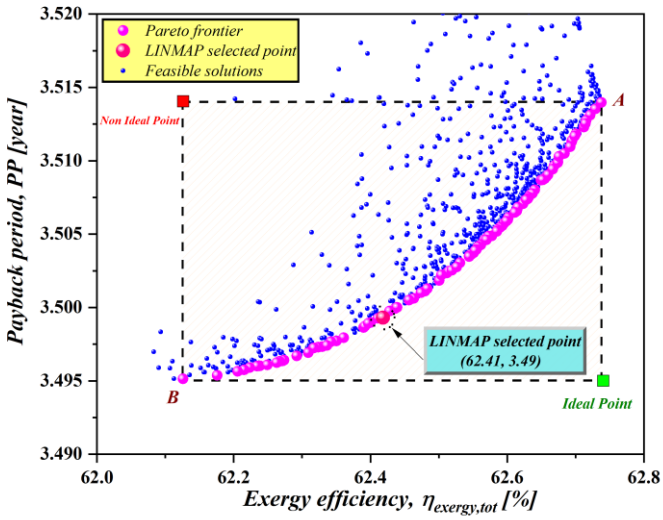

Fig. 4. The Pentane/Butane zeotropic mixture optimization result.

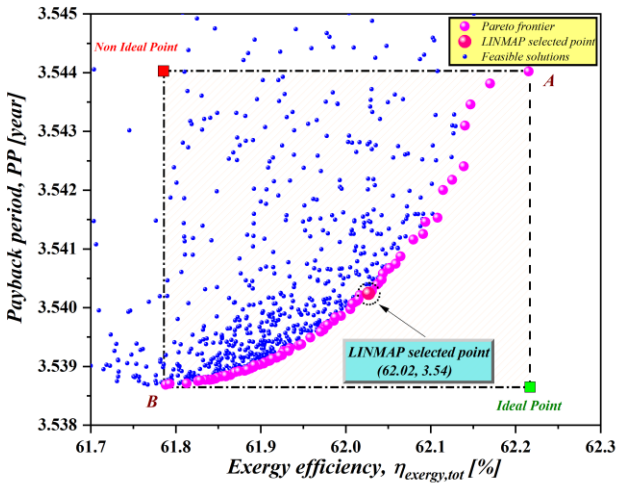

Fig. 5. The Pentane/Cis-2-butene zeotropic mixture optimization result.

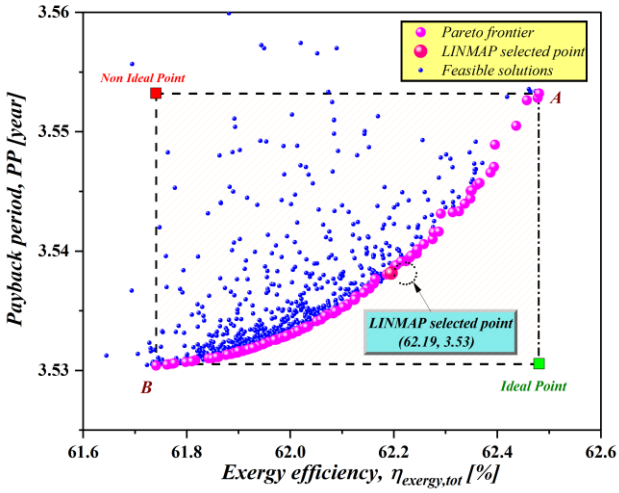

Fig. 6. The Pentane/Hexane zeotropic mixture optimization result.

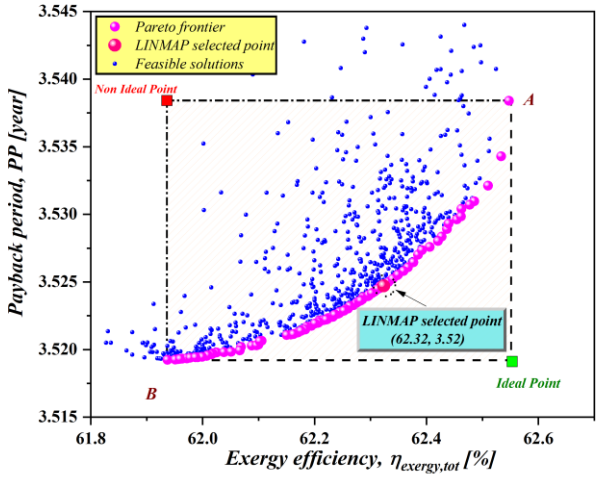

Fig. 7. The Pentane/Trans-2-butene zeotropic mixture optimization result.

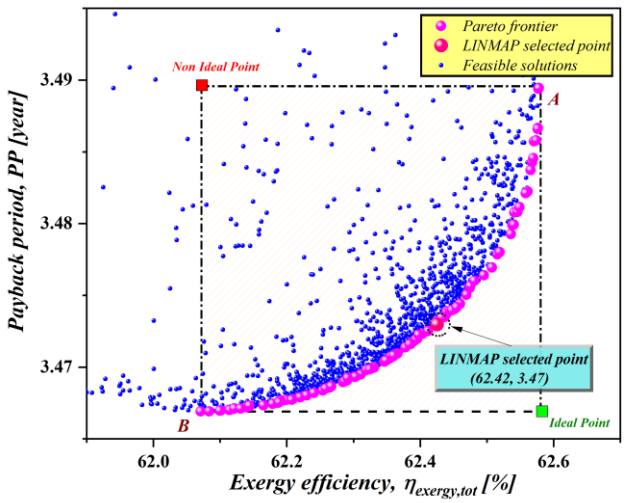

Fig. 8. The Perfluoropentane/Butene zeotropic mixture optimization result.

6.2. *The DORC subsystem's working fluid selection*

In the previous section, the optimum state of the proposed system with the considered zeotropic mixtures was evaluated, and based on their results, the other performance criteria were calculated. In this section, the total and DORC subsystem net power, exergy destruction, thermal efficiency, and exergetic efficiency are compared, and the DORC subsystem working fluid selection is performed.

5.2.1. *The net output power comparison*

The DORC subsystem and the comparison of the considered zeotropic mixture's total net power generation are shown in Figs. 9a and 9b, respectively. Perfluoropentane/butene shows the most excellent DORC net power at about 2306.94 kW. At the same time, pentane/butane offers the highest net power for the DORC subsystem at approximately 2234.18 kW, as shown in Fig. 9a. Isopentane/Butane provides the DORC's required minimum net power, approximately 2077.73 kW. Fig. 9b compares the total net power of the suggested system for various zeotropic mixtures. Similar to the DORC pattern, the perfluoropentane/butene mixture has the highest net power at around 7992.29 kW, while isopentane/butane has the lowest net power at approximately 7763.08 kW. The total and DORC net power differences are the same in any zeotropic mixture. Therefore, it can be said that the working fluid of the DORC subsystem has no effect on the geothermal system's net power generation.

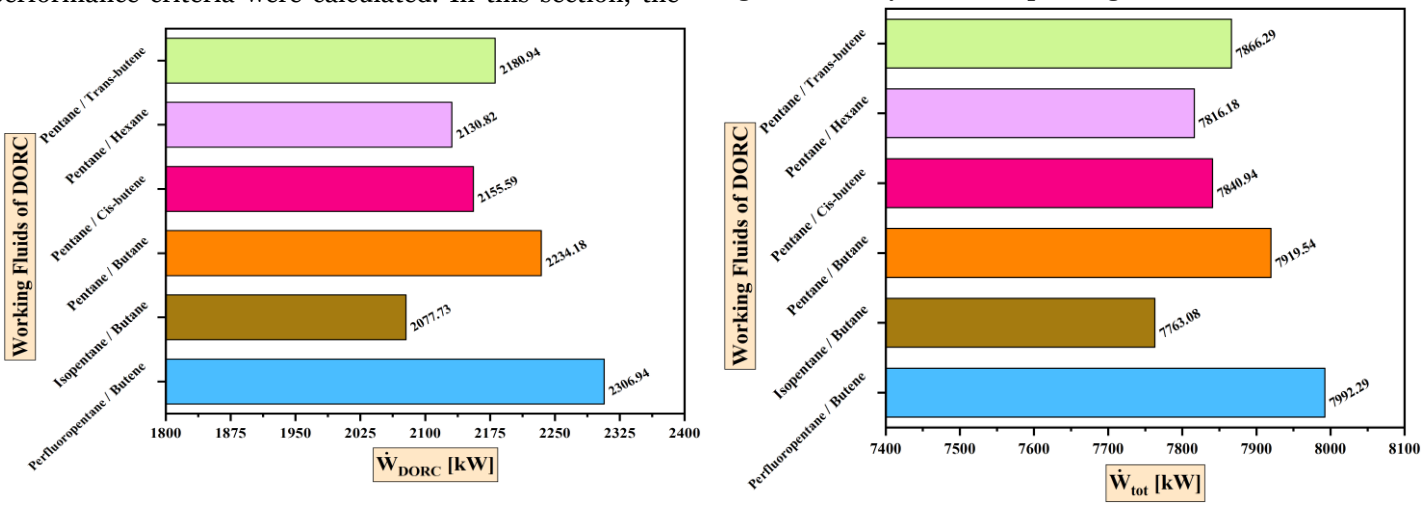

(a) (b)

Fig. 9. The total and DORC subsystem net power production comparison.

5.2.2. *The exergy destruction comparison*

Fig. 10a illustrates the comparison of DORC subsystem exergy destruction with different working fluids. The maximum exergy destruction belongs to the perfluoropentane/butene mixtures (about 2328.4 kW), and the following most exergy-destroying mixture is pentane/cis-2-butene. The pentane/hexane includes the minimum exergy destruction of about 2241.52 kW. Also, the pentane/butane are placed in the fourth stage of the exergy destroyer mixture, and the second high net power belongs to this mixture. The total exergy destruction of the different zeotropic mixtures is compared in Fig. 10b, in which the perfluoropentane/butene presents the highest exergy destruction of about 4810.7 kW and the pentane/hexane presents the minimum exergy destruction of about 4751 kW. Focusing on the total and DORC subsystem exergy destruction differences demonstrates that the DORC working fluid influences the geothermal system's exergy destruction so that this difference varies between the mixtures. Because the DORC working fluid

affects the vapor generators 1 and 2, and the Hx unit's exergy balance.

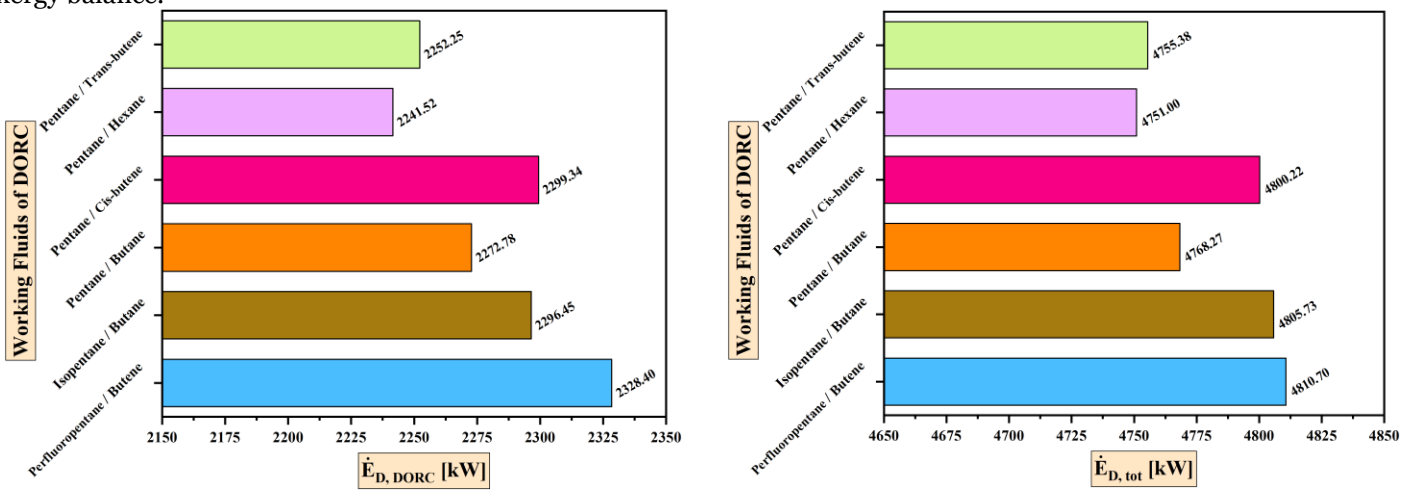

(a) (b)

Fig. 10. The comparison of the total and DORC subsystem exergy destruction.

5.2.3. The energetic efficiency comparison

The energy efficiency comparison of the DORC subsystems for the selected DORC working fluids is shown in Fig. 11a. According to the results in Fig. 11a, the pentane/trans-2-butene mixture shows the DORC subsystem's maximum energy efficiency at around 12.08%, and the isopentane/butane mixture shows its minimum energetic efficiency at about 11.75%. Although perfluoropentane/butene has the maximum net power for the DORC, getting this mixture to the right temperature for the turbine takes more energy. As a result, this mixture, which is in the fourth stage, has a lower energy efficiency of roughly 11.89%. The outcomes for overall energetic efficiency vary. According to Fig. 11b, pentane/hexane exhibits the highest overall energy efficiency, around 18.37%, whereas this mixture's DORC energetic efficiency and pentane/butane were both equal. Additionally, the isopentane/butane mixture, which exhibits the minimum DORC energetic efficiency and has a total energy efficiency of 18.24%, is situated at the third stage. Also, the mix of perfluoropentane/butane has the lowest energy efficiency, roughly 18.05 percent. These findings show that, in contrast to the net power trend, the DORC subsystem working fluid significantly affects the proposed system's overall energy efficiency.

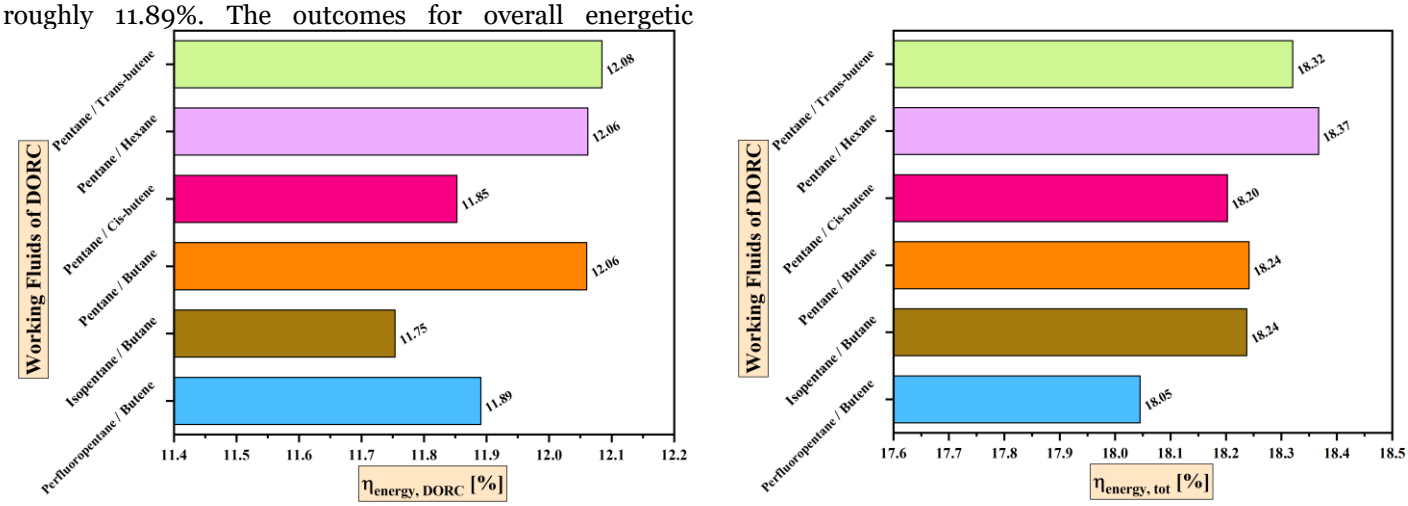

(a) (b)

Fig. 11. The comparison of the total and DORC subsystem energetic efficiency.

5.2.4. The exergetic efficiency comparison

Fig. 12 illustrates the total and DORC subsystem exergetic efficiency comparisons between candidates' working fluids. Fig. 12a shows that the perfluoropentane/butene mixture provides the highest DORC exegetic efficiency, about 49.77%. This zeotropic

mixture includes the maximum net power and exergy destruction among the considered zeotropic mixtures. But the net power effect on the exergetic efficiency overcomes the exergy destruction effect. Also, the isopentane/butane mixture presents the lowest exergetic efficiency for the DORC subsystem because this mixture has the lowest net power and high exergy efficiency. The total exergetic efficiency comparison is presented in Fig. 12b. Regarding the obtained results, the perfluoropentane/butene mixture presents the highest total exergetic efficiency, about 62.43%, and the pentane/butane mixture presents 62.42% total exergetic efficiency, which is too close to the perfluoropentane/butene and is placed in the second stage. The isopentane/butane mixture provides the minimum total exergetic efficiency of about 61.76%.

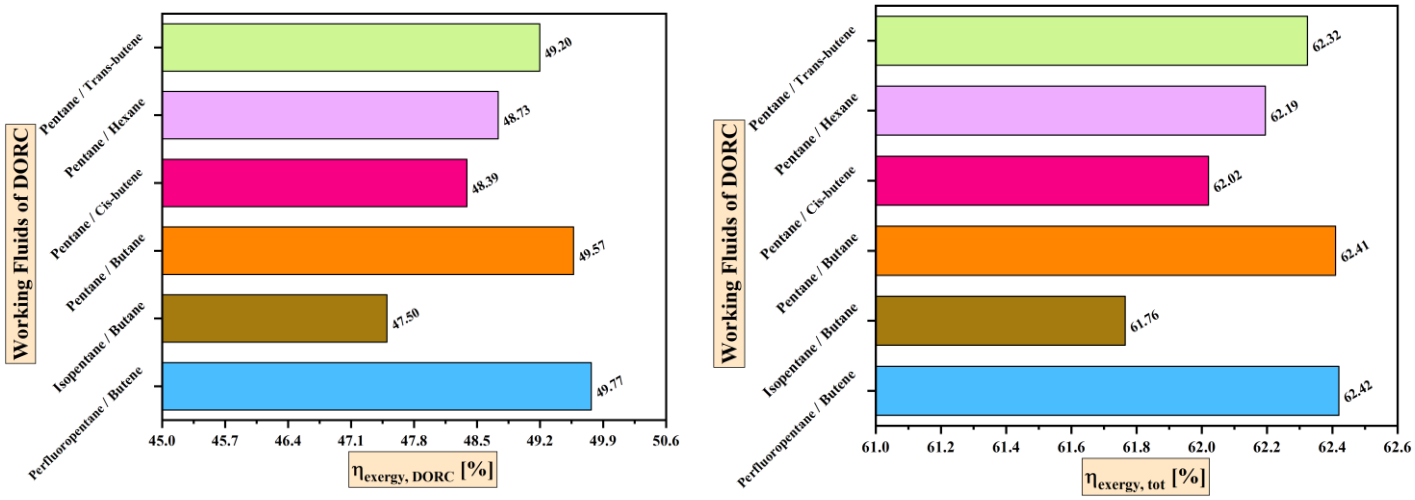

(a) (b)

Fig. 12. The comparison of the total and DORC subsystem energetic efficiency.

The comparison of the proposed system and DORC subsystem performance criteria with the obtained payback period for the different zeotropic mixtures leads to the selection of the perfluoropentane/butene mixture as the best working fluid for the DORC subsystem. This mixture provides the highest net power and exergetic efficiency and the lowest payback period among the considered zeotropic mixtures. If only the energy approach were the paper assessment for the proper working fluid selection of the DORC subsystem, the pentane/hexane mixture would be the best working fluid for the DORC subsystem. Hence, the forward section results are based on the perfluoropentane/butene mixture as the DORC subsystem working fluid.

6.3. The net present value evaluation

The NPV estimation evaluates the proposed system's payback period and profitability over its designed lifetime. Also, it shows the financial roadmap of the system's economic approach. In this way, in this section, the NPV of the proposed system is estimated for four different geofluid and electric sale prices. Fig. 13 shows the NPV of the proposed system for the four different scenarios of geofluid and electricity sale prices at the optimum operational condition. In the first scenario, the geofluid and electricity sale prices are assumed to be about 1.3 $/GJ and 0.08 $/kWh, respectively. At these prices, the proposed system's payback period is about 3.47 years, and the system presents a 10.85 M$ net profit. In the second scenario, the geofluid price is considered 1.7 $GJ, and the electricity sale price is assumed to be 0.06 $/kWh. At this sale and incoming price scenario, the payback period is about 19.77 years with a 0.06 M$ net profit during the 20-year system's lifetime. The geofluid and electricity sale prices in the third scenario are considered to be 1.7 $/GJ and 0.08 $/kWh, respectively. At these prices, the proposed system's payback period is about 4.47 years, and the system presents a 7.06 M$ net profit. Finally, in the fourth NVP estimation scenario, the electricity sale price and geofluid price are assumed to be about 0.1 $/kWh and 1.3 $/GJ respectively. At these considered prices the proposed system payback period and net profit are obtained about 2.62 years and 17.85 M$. Comparing the second and third NPV estimation scenarios demonstrates that increasing the electricity sale prices by about 33%, improves the payback by approximately 77.38% and presents a 11660% higher net

profit. Also, increasing the electricity prices by about 25% presents a 22.9% lower payback period and 64.51% more net profit (comparison of the first and fourth scenarios). Furthermore, the third and first scenarios NPV estimation comparison illustrates that increasing the geofluid price by about 30.76% increases the payback period by approximately 31.47% and reduces the system net profit by approximately 34.93%.

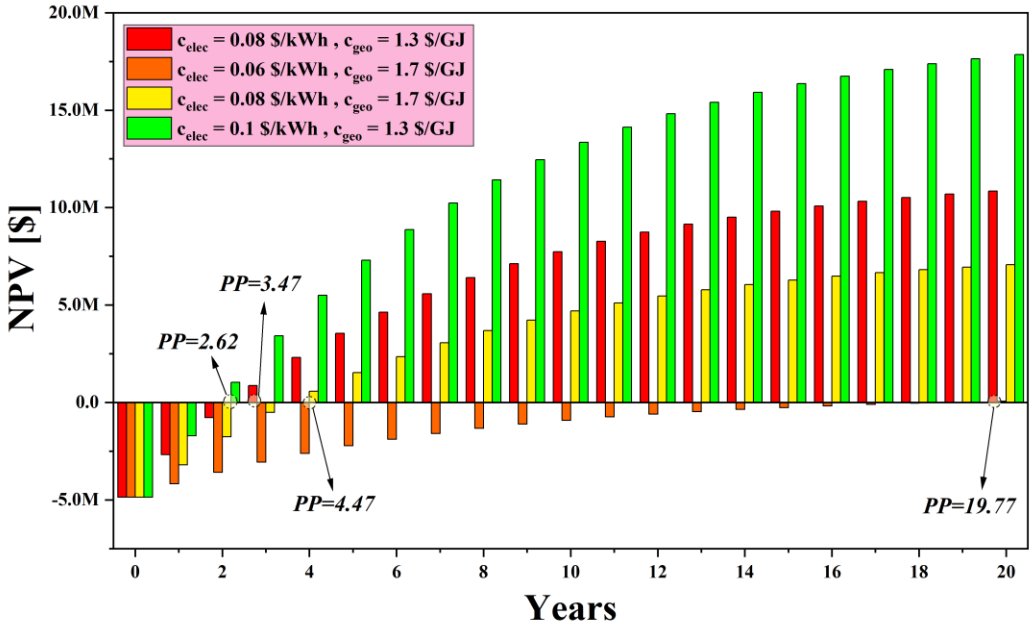

Fig. 13. The net present value estimation for the four different prices at the optimum operational condition.

6.4. The Grassmann diagram

The total exergy destruction distribution in the system components is presented in Fig. 14 as a Grassmann diagram. The Grassmann diagram's information shows that the steam turbine unit contains 966 kW of exergy destruction, which is the maximum exergy destruction between the system's components. The following components with the highest exergy destruction are the first expansion valve and condenser 1, at about 714 and 671 kW, respectively. Also, the separation tanks present zero exergy destruction. Since the vapor generators inlet mass flow rates are lower than the Hx unit in the DORC subsystem, the Hx unit contains higher exergy destruction than the vapor generator units. Focusing on the overall exergy destruction distribution reveals that the employed condensers include the highest portion of the total exergy destruction by about 26.98%. Also, the steam turbine unit, as the highest exergy destroyer component, contains 20% of the total exergy destruction in the proposed system, and the condenser 2 has the highest exergy destruction in the DORC subsystem at about 627 kW.

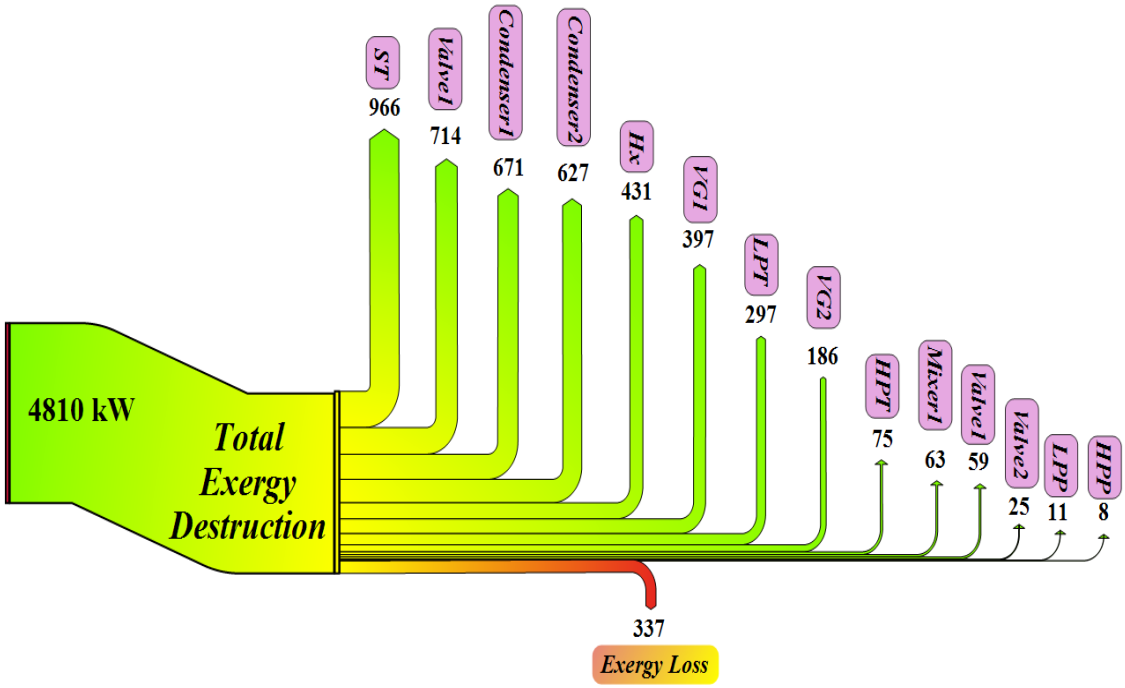

Fig. 14. The Grassmann diagram of the proposed system at the optimum operational condition.

7. Conclusion

In this paper, a geothermal power system is proposed to generate power. Also, a DORC subsystem with the zeotropic working fluid was employed to recover the geothermal system's waste energy and generate more power. Comprehensive mass, energy, exergy, and exergoeconomic analyses were applied to evaluate the proposed system's performance. Six different zeotropic mixtures were considered the DORC subsystem's working fluid. Then, the DORC subsystem's working fluid selection was conducted by comparing their performance at the optimum state. Also, the NPV index evaluation was performed for the four different electricity sales and geofluid prices. Finally, the exergy destruction distribution of the proposed system is shown as the Grassmann diagram. All studies conducted led to the following conclusions:

- The perfluoropentane/butene mixture presents the highest net power, exergetic efficiency, and lowest payback period. So, it is selected as the DORC subsystem's working fluid.
- Employing the DORC subsystem to recover the proposed geothermal power system generates 2306.94 kW more power.
- The proposed system can produce 7992.29 kW of net power with 62.42% exergetic efficiency and a 3.47 years payback period.
- The DORC working fluid does not influence the geothermal system's power production, but it influences the exergy destruction and energetic and exergetic efficiencies of the geothermal system.
- The electricity cost impacts the NPV index more than the geofluid cost.
- The steam turbine accounts for 20% of the total exergy destruction in the proposed system.

For future work, other different zeotropic mixtures can be considered the working fluid of the DORC subsystem, and their performance in different modes can be compared.

REFERENCES

[1] A. G. Olabi, M. Mahmoud, B. Soudan, T. Wilberforce, and M. Ramadan, "Geothermal based hybrid energy systems, toward eco-friendly energy approaches," *Renew Energy*, vol. 147, pp. 2003–2012, 2020.

[2] H. Tian, L. Chang, Y. Gao, G. Shu, M. Zhao, and N. Yan, "Thermo-economic analysis of zeotropic mixtures based on siloxanes for engine waste heat recovery using a dual-loop organic Rankine cycle (DORC)," *Energy Convers Manag*, vol. 136, pp. 11–26, 2017.

[3] M. Malik, I. Dincer, and M. A. Rosen, "Development and analysis of a new renewable energy-based multi-generation system," *Energy*, vol. 79, pp. 90–99, 2015.

[4] A. Habibollahzade, Z. K. Mehrabadi, and C. N. Markides, "Comparative thermoeconomic analyses and multi-objective particle swarm optimization of geothermal

combined cooling and power systems," *Energy Convers Manag*, vol. 234, p. 113921, 2021.
[5] F. A. Boyaghchi and P. Heidarnejad, "Thermoeconomic assessment and multi objective optimization of a solar micro CCHP based on Organic Rankine Cycle for domestic application," *Energy Convers Manag*, vol. 97, pp. 224–234, 2015.
[6] J. Song, P. Loo, J. Teo, and C. N. Markides, "Thermo-economic optimization of organic Rankine cycle (ORC) systems for geothermal power generation: A comparative study of system configurations," *Front Energy Res*, vol. 8, p. 6, 2020.
[7] W. E. Glassley, *Geothermal energy: renewable energy and the environment*. CRC press, 2014.
[8] S. J. Zarrouk and M. H. Purnanto, "Geothermal steam-water separators: Design overview," *Geothermics*, vol. 53, pp. 236–254, 2015.
[9] Z. Guzović, B. Majcen, and S. Cvetković, "Possibilities of electricity generation in the Republic of Croatia from medium-temperature geothermal sources," *Appl Energy*, vol. 98, pp. 404–414, 2012.
[10] C. Luo, L. Huang, Y. Gong, and W. Ma, "Thermodynamic comparison of different types of geothermal power plant systems and case studies in China," *Renew Energy*, vol. 48, pp. 155–160, 2012.
[11] M. Yari, "Exergetic analysis of various types of geothermal power plants," *Renew Energy*, vol. 35, no. 1, pp. 112–121, 2010.
[12] M. Abdolalipouradl, F. Mohammadkhani, and S. Khalilarya, "A comparative analysis of novel combined flash-binary cycles for Sabalan geothermal wells: Thermodynamic and exergoeconomic viewpoints," *Energy*, vol. 209, p. 118235, 2020.
[13] S. M. Bina, S. Jalilinasrabady, and H. Fujii, "Thermo-economic evaluation of various bottoming ORCs for geothermal power plant, determination of optimum cycle for Sabalan power plant exhaust," *Geothermics*, vol. 70, pp. 181–191, 2017.
[14] N. A. Pambudi, R. Itoi, S. Jalilinasrabady, and K. Jaelani, "Performance improvement of a single-flash geothermal power plant in Dieng, Indonesia, upon conversion to a double-flash system using thermodynamic analysis," *Renew Energy*, vol. 80, pp. 424–431, 2015.
[15] A. D. Pasek, T. A. F. Soelaiman, and C. Gunawan, "Thermodynamics study of flash–binary cycle in geothermal power plant," *Renewable and sustainable energy reviews*, vol. 15, no. 9, pp. 5218–5223, 2011.
[16] N. Shokati, F. Ranjbar, and M. Yari, "Exergoeconomic analysis and optimization of basic, dual-pressure and dual-fluid ORCs and Kalina geothermal power plants: A comparative study," *Renew Energy*, vol. 83, pp. 527–542, 2015.
[17] A. Franco and M. Villani, "Optimal design of binary cycle power plants for water-dominated, medium-temperature geothermal fields," *Geothermics*, vol. 38, no. 4, pp. 379–391, 2009.
[18] B. Peris, J. Navarro-Esbrí, and F. Molés, "Bottoming organic Rankine cycle configurations to increase Internal Combustion Engines power output from cooling water waste heat recovery," *Appl Therm Eng*, vol. 61, no. 2, pp. 364–371, 2013.
[19] J. Li, Z. Ge, Y. Duan, Z. Yang, and Q. Liu, "Parametric optimization and thermodynamic performance comparison of single-pressure and dual-pressure evaporation organic Rankine cycles," *Appl Energy*, vol. 217, pp. 409–421, 2018.
[20] Z. Ge, J. Li, Q. Liu, Y. Duan, and Z. Yang, "Thermodynamic analysis of dual-loop organic Rankine cycle using zeotropic mixtures for internal combustion engine waste heat recovery," *Energy Convers Manag*, vol. 166, pp. 201–214, 2018.
[21] W. Li, X. Feng, L. J. Yu, and J. Xu, "Effects of evaporating temperature and internal heat exchanger on organic Rankine cycle," *Appl Therm Eng*, vol. 31, no. 17–18, pp. 4014–4023, 2011.
[22] L. Zhao and J. Bao, "Thermodynamic analysis of organic Rankine cycle using zeotropic mixtures," *Appl Energy*, vol. 130, pp. 748–756, 2014.
[23] J. Wang, J. Wang, Y. Dai, and P. Zhao, "Thermodynamic analysis and optimization of a flash-binary geothermal power generation system," *Geothermics*, vol. 55, pp. 69–77, 2015.
[24] A. Sohani, H. Sayyaadi, and M. Zeraatpisheh, "Optimization strategy by a general approach to enhance improving potential of dew-point evaporative coolers," *Energy Convers Manag*, vol. 188, pp. 177–213, 2019.
[25] H. Rostamzadeh, M. Ebadollahi, H. Ghaebi, and A. Shokri, "Comparative study of two novel micro-CCHP systems based on organic Rankine cycle and Kalina cycle," *Energy Convers Manag*, vol. 183, pp. 210–229, 2019.
[26] T. Parikhani, J. Jannatkhah, A. Shokri, and H. Ghaebi, "Thermodynamic analysis and optimization of a novel power generation system based on modified Kalina and GT-MHR cycles," *Energy Convers Manag*, vol. 196, pp. 418–429, 2019.
[27] Y. A. Cengel, M. A. Boles, and M. Kanoğlu, *Thermodynamics: an engineering approach*, vol. 5. McGraw-hill New York, 2011.
[28] Y. Jaluria, *Design and optimization of thermal systems*. CRC press, 2007.
[29] Y. Zhou, S. Li, L. Sun, S. Zhao, and S. S. A. Talesh, "Optimization and thermodynamic performance analysis of a power generation system based on geothermal flash and dual-pressure evaporation organic Rankine cycles using zeotropic mixtures," *Energy*, vol. 194, p. 116785, 2020.